

## Sulfate adsorption at the buried hematite/solution interface investigated using total internal reflection (TIR)-Raman spectroscopy

Aaron M. Jubb<sup>a,1</sup>, Dominique Verreault<sup>a</sup>, Ralf Posner<sup>a,b,2</sup>, Louise J. Criscenti<sup>c</sup>, Lynn E. Katz<sup>d</sup>, Heather C. Allen<sup>a,\*</sup>

<sup>a</sup> Department of Chemistry and Biochemistry, The Ohio State University, 100 West 18th Avenue, Columbus, OH 43210, USA

<sup>b</sup> Department of Materials Science and Engineering, The Ohio State University, 2041 College Road, Columbus, OH 43210, USA

<sup>c</sup> Geochemistry Department, Sandia National Laboratories, P.O. Box 5800, MS 0754, Albuquerque, NM 87109, USA

<sup>d</sup> Department of Civil, Architectural and Environmental Engineering, College of Engineering, The University of Texas at Austin, 1 University Station C1700, Austin, TX 78712, USA

### ARTICLE INFO

#### Article history:

Received 11 January 2013

Accepted 18 February 2013

Available online 6 March 2013

#### Keywords:

Surface spectroscopy

Silica

Hematite

Adsorption

Inner-sphere

### ABSTRACT

Sulfate adsorption at buried mineral/solution interfaces is of great interest in geochemistry and atmospheric aerosol chemistry due to the sulfate anion's environmental ubiquity and the wide role of physical and chemical phenomena that it impacts. Here we present the first application of total internal reflection-Raman (TIR-Raman) spectroscopy, a surface-sensitive spectroscopy, to probe sulfate ion behavior at the buried hematite/solution interface. Hematite is the most thermodynamically stable iron oxide polymorph and as such is widely found in nature. Our results demonstrate the feasibility of a TIR-Raman approach to study simple, inorganic anion adsorption at buried interfaces. Moreover, our data suggest that inner-sphere sulfate adsorption proceeds in a bidentate fashion at the hematite surface. These results help clarify long-standing questions as to whether sulfate forms inner-sphere adsorption complexes at hematite surfaces in a mono- or bidentate fashion based on attenuated total reflection-infrared (ATR-IR) observations. Our results are discussed with perspective to this debate and the applicability of TIR-Raman spectroscopy to address ambiguities of ion adsorption to mineral surfaces.

© 2013 Elsevier Inc. All rights reserved.

### 1. Introduction

Ion interactions with solid surfaces at buried mineral/solution interfaces are vital to understand in order to predict the mobility and fate of aqueous contaminants within the environment [1]. Oxide minerals form the major components of Earth's upper continental crust, with silicon, aluminum, and iron oxides being the most predominant [2]. Due to the high prevalence of oxide minerals, rationalizing ion interactions with their surfaces is critical for predicting the spatial distribution of ions in subsurface environments through time. Oxide minerals also make up the majority of mineral dust aerosols and ion interactions at their surfaces have been demonstrated to influence their chemical and physical properties [2,3]. Hematite ( $\alpha$ -Fe<sub>2</sub>O<sub>3</sub>) is the most thermodynamically stable iron oxide polymorph and, as such, is found globally within

soil, water, and atmospheric systems [2,4]. Recognizing the environmental importance of hematite, numerous experimental and computational studies have been performed to understand the properties of hematite/aqueous interfaces in detail [5–14]. However, many questions remain as to the structure (binding mode) and energetics of ion adsorption on hematite.

One of the most prevalent inorganic anions in the environment is sulfate ( $\text{SO}_4^{2-}$ ). It is the third most abundant inorganic ion within seawater by mass [15] and the end oxidation product of sulfur containing compounds [16,17]. Due to its environmental ubiquity sulfate has been extensively studied both in the geochemical and atmospheric communities. Particularly in aqueous geochemistry, sulfate adsorbate structure on a wide variety of mineral substrates has been the focus of many experimental and theoretical studies seeking to understand and rationalize ion mobility and transport [5,6,8,10,11,18–20]. In addition, heavy metals may adsorb to mineral surfaces concurrent with sulfate forming ternary complexes [21–23]. For instance, Rose and Bianchi-Mosquera showed that hematite in contact with red-bed pore fluids rich in chloride and sulfate may lead to the separation of Cu and Ag to form stratiform Cu deposits during diagenesis [24]. Sulfate has also been demonstrated to play an important role in the atmospheric chemistry of aerosols. For example, sulfate coatings on mineral dust aerosols

\* Corresponding author.

E-mail address: allen@chemistry.ohio-state.edu (H.C. Allen).

URL: <http://research.chemistry.ohio-state.edu/allen> (H.C. Allen).

<sup>1</sup> Current address: Earth System Research Laboratory, Chemical Sciences Division, National Oceanic and Atmospheric Administration and the Cooperative Institute for Research in Environmental Sciences, University of Colorado, Boulder, CO 80305, USA.

<sup>2</sup> Current address: Henkel AG & Co. KGaA, Henkelstrasse 67, 40589 Düsseldorf, Germany.

significantly decrease their ice nucleation abilities which may impact cirrus cloud formation [3,25]. Secondary organic aerosol (SOA) formation has also been linked to the seed aerosol sulfate content [26,27].

The most common in situ spectroscopic techniques for probing ion interactions at buried mineral oxide/solution interfaces are attenuated total reflection-infrared (ATR-IR) and X-ray absorption spectroscopies [5,19,28–31]. The spectroscopic results thus obtained provide benchmarks for modeling efforts that ultimately lead to the prediction of contaminant transport. Thus it is vital that ion adsorption structures at oxide surfaces interpreted from spectroscopic results are correct in order to facilitate accurate models [8–10,32].

The use of ATR-IR spectroscopy to measure the in situ adsorption structure of sulfate at the hematite surface was first demonstrated by Hug in 1997 [5]. This method takes advantage of the symmetry lowering effects caused by  $\text{SO}_4^{2-}$  anion adsorption which breaks the triple degeneracy of  $T_d$   $\text{SO}_4^{2-}$  ion asymmetric stretching ( $\nu_{\text{AS}}\text{-SO}_4^{2-}$ ) modes. If the adsorbed  $\text{SO}_4^{2-}$  ion has bound to the surface with one oxygen ligand (monodentate binding) the resulting symmetry will be lowered to  $C_{3v}$  and two  $\nu_{\text{AS}}\text{-SO}_4^{2-}$  peaks are expected in the IR spectra. When  $\text{SO}_4^{2-}$  inner-sphere adsorption involves two of the sulfate's oxygen ligands (bidentate binding) the symmetry of the adsorbed  $\text{SO}_4^{2-}$  ion will further lower to  $C_{2v}$  which will completely lift the  $\nu_{\text{AS}}\text{-SO}_4^{2-}$  degeneracy such that three distinct  $\nu_{\text{AS}}\text{-SO}_4^{2-}$  peaks can be expected. Hug's approach has been widely adopted to probe adsorption of sulfate, as well as adsorption of many other inorganic ions, to a large variety of mineral surfaces, including hematite [5,6,18,19,33].

However, a general drawback of using ATR-IR spectroscopy to study ion adsorption at mineral/solution interfaces is that the penetration depth for the IR evanescent wave is generally on the order of microns [34–37]. This signifies that for studies using ATR-IR spectroscopy to probe ion adsorption at mineral surfaces signal contributions arise not only from adsorbed surface species, but also from ions residing in the interfacial electric double layer and bulk solvated ions. As a result sulfate inner-sphere adsorption geometries inferred from these spectra may be questioned due to the potentially weak spectral features being obscured by signal arising from bulk solvated sulfate species.

In contrast to an ATR-IR approach, the Raman counterpart, total internal reflection-Raman (TIR-Raman) spectroscopy, has yet to be adopted in the study of ion interactions at mineral/solution interfaces. Only recently has TIR-Raman spectroscopy been applied to study adsorption onto mineral surfaces, most notably by Bain and co-workers, and these studies primarily focused on organic molecule adsorption [36,38–40]. The TIR-Raman approach has the main advantage over ATR-IR in that the attainable penetration depth is much less ( $\sim 40\text{--}300\text{ nm}$ ) owing to the much shorter excitation wavelengths used [41,42].

Here we present, to the authors' knowledge, the first application of TIR-Raman spectroscopy to study simple inorganic ion adsorption at buried mineral/solution interfaces. In this study  $\text{SO}_4^{2-}$  ion interactions at the hematite/solution interface are examined as a function of ion concentration and pH. Our results demonstrate that a bidentate geometry for  $\text{SO}_4^{2-}$  inner-sphere adsorption onto the hematite surface is dominant, in agreement with recent work by Paul et al. [18] and Rubasinghege et al. [43], for the conditions tested. These results lend support to proposed bidentate adsorption structures for sulfate at hematite surfaces inferred by Paul et al. from ATR-IR spectra and modeling results in contrast to a monodentate adsorption motif previously put forward by several other groups [5,6].

## 2. Experimental methods and materials

TIR-Raman spectroscopy is analogous to conventional Raman spectroscopy in that it relies upon the detection of inelastic scattered light. However, in TIR-Raman spectroscopy the detected scattered light originates from an evanescent wave generated when light propagating through an optically denser medium is incident upon an interface with an optically rarer medium at or above the critical angle ( $\theta_{i,c}$ ) defined by

$$\theta_{i,c} = \arcsin\left(\frac{n_2}{n_1}\right), \quad (1)$$

where  $n_1$  and  $n_2$  refers to the refractive indices of the optically denser and rarer media, respectively. The distance from the interface into the second medium at which the amplitude of the evanescent field decays to  $1/e$  of its maximum value is called the penetration depth ( $d_p$ ) and is defined by [34,37]

$$d_p = \frac{\lambda}{2\pi\sqrt{n_1^2 \sin^2 \theta_i - n_2^2}}, \quad (2)$$

where  $\lambda$  is the wavelength in vacuum and  $\theta_i$  is the incident angle from the surface normal of the input beam. From Eq. (2) it can be shown that the penetration depth of TIR-Raman will generally be on the order of 100 nm with a 532.1 nm excitation wavelength for a typical oxide mineral/water interface at the critical angle, i.e. at least one order of magnitude smaller than the probing distance of a typical ATR-IR experiment. This indicates that TIR-Raman should serve as an effective probe of surface processes such as ion adsorption.

Fig. 1 gives a schematic representation of the custom-built TIR-Raman spectrometer setup used in this study. The excitation source for the TIR-Raman instrument is a diode-pumped Nd:YVO<sub>4</sub> laser (Millennium II, Spectra-Physics) which produces single-mode (TEM<sub>00</sub>), *p*-polarized ( $>100:1$  polarization ratio), 532.1 nm (second harmonic) continuous-wave light with output energies of up to 2 W. However, for all spectra presented in this study the laser was operated with an output energy of 200 mW and the excitation beam was further attenuated to  $\sim 40\text{ mW}$  by a neutral density filter before the sample flow cell to reduce hematite thin film ablation by

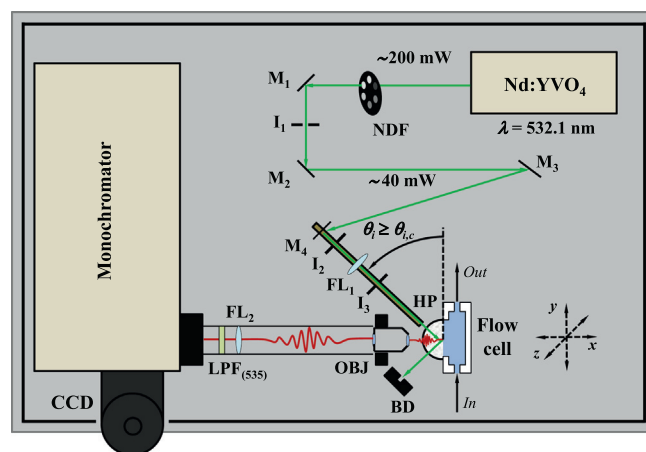


**Fig. 1.** Schematic representation of the TIR-Raman setup. The input beam goes through several optical components including a neutral density filter (NDF) wheel, Ag mirrors (M), irises (I), focusing lenses (FL) before reaching the planar face of a hemispherical prism (HP). The reflection of the input beam is directed to a beam dump (BD). The Raman scattered beam generated at the prism/solution interface is collected by a microscope objective (OBJ) and filtered by a 535 nm longpass filter (LPF) before entering the monochromator.

the laser beam. Thin film ablation was an issue for higher input laser powers due to the intense coloring of the hematite films. The beam was directed to the sample flow cell by a series of four silver mirrors and focused onto the mineral/solution interface via a 5 cm focal lens. The last mirror and focal lens are mounted on a manually controllable goniometer arm in order to achieve the desired incident beam angle. All spectra were collected with an incident beam angle of  $75^\circ$  from the surface normal, thus exceeding the critical angle of the silica/solution ( $\theta_{i,c} \approx 66.3^\circ$ ) interface. The penetration depth with this geometry was  $\sim 185$  nm at 532.1 nm for the silica/solution interface. As for the hematite-coated silica/solution interface, the value of the penetration depth is more difficult to determine, partly because few data are available about the optical constants of deposited hematite thin films [44,45]. Moreover, it is recognized that these optical constants can differ from their bulk values as they depend strongly on the deposition conditions (e.g. temperature). However, if an average refractive index value of 2.9 is assumed for most hematite film thicknesses, then the effective penetration depth into the solution at 532.1 nm for this input geometry will be approximately 34 nm.

A  $50\times$  objective lens (infinity-corrected, super-long working distance (13.8 mm), 0.45 numerical aperture, Nikon) mounted normal to the center of the TIR element and centered in front of the excitation beam spot was used to collect the TIR-Raman scatter. This objective lens is also mounted on an  $x$ - $y$ - $z$  translational stage to ease alignment and to allow greater collection efficiency of the generated TIR-Raman signal. The collected TIR-Raman scatter was focused (7 cm focal length) and then separated from the 532.1 nm Rayleigh scatter by using a 535 nm longpass filter (Omega Optical, Custom) before entering a monochromator (SpectraPro 500i, Princeton Instruments) equipped with a 1200 groove/mm grating and detected on a liquid  $N_2$ -cooled deep-depletion CCD (1340/400 EB, Roper Scientific) calibrated against the 435.833 nm emission line of a fluorescent Hg lamp.

The sample flow cell was custom-made from Teflon with aluminum mounts to clamp a hemispherical TIR element onto the sample flow cell reservoir with its planar side exposed to the aqueous solution. This flow cell was mounted on an  $x$ - $y$ - $z$  translational stage. Solution inflow and outflow are supplied by a peristaltic pump (MasterFlex L/S, Cole-Parmer).

The TIR-Raman experiments were carried out using a bare fused silica hemisphere (25.4 mm diameter  $\times$  12.7 mm height, surface quality 60/40, ISP Optics Inc.) or a 100 nm-thick hematite-coated fused silica hemisphere as the TIR element. All fused silica hemispheres were cleaned before use or before thin film deposition by soaking in a mixture of concentrated sulfuric acid (certified ACS Plus, Fisher Scientific) and ammonium peroxydisulfate (crystalline, certified ACS, Fisher Scientific) for at least 4 h followed by copious rinsing with nanopure water (18.3 M $\Omega$ , NanoPure, Barnstead/ThermoFyne) [46]. The silica hemispheres were then sonicated in dry methanol (reagent grade, Sigma-Aldrich) for at least 1 h, thoroughly rinsed with nanopure water and dried under a stream of house  $N_{2(g)}$ . The hematite thin film synthesis was carried out according to the procedure of Jubb and Allen and resulted in polycrystalline thin films of homogeneous hematite phase as determined by Raman microscopy [47]. Raman spectra of a typical hematite film coated on a silica hemisphere were obtained using a Renishaw inVia Raman microscope with a  $50\times$  objective coupled to a 632.8 nm He-Ne laser excitation source (Renishaw RL633). The laser power at the sample was approximately 6 mW. The resolution of this instrument was approximately  $3\text{ cm}^{-1}$  with an 1800 grooves/mm grating. Fig. 2 shows the Raman spectrum and an optical image (see inset) of the hematite film used in this study where all seven diagnostic Raman modes of hematite are clearly identifiable with no spectral signatures of other oxide phases present [47,48].

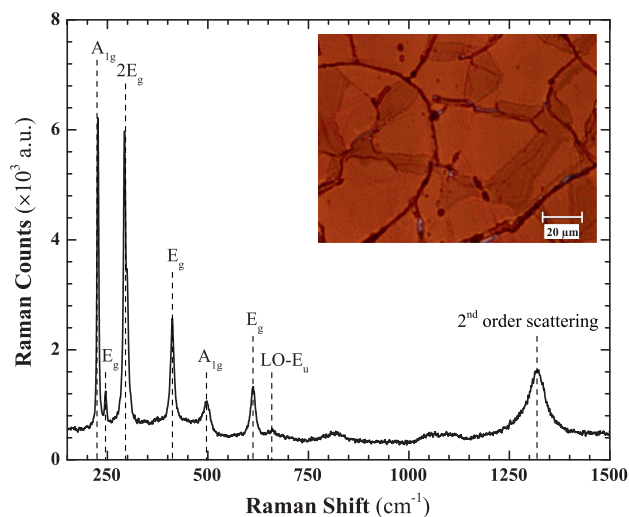


**Fig. 2.** Raman spectrum of a typical  $\sim 100$  nm-thick hematite film coated on a silica hemisphere collected with a 632.8 nm He-Ne laser excitation source ( $\sim 6$  mW) through a  $50\times$  objective lens. Peak centers are indicated by dashed vertical lines and mode assignments are given [47]. The seven diagnostic Raman peaks of hematite are clearly present as well as the LO- $E_u$  mode at  $660\text{ cm}^{-1}$  and the second-order scattering peak at  $1318\text{ cm}^{-1}$ . The broad, weakly defined peaks at  $\sim 800\text{ cm}^{-1}$  and  $1075\text{ cm}^{-1}$  are also present in many published Raman spectra of hematite. Inset is an optical image of the hematite film.

All silica/solution TIR-Raman spectra were collected with 90 s acquisition times. The hematite-coated silica/solution spectra shown are the average of nine 2 min acquisitions. For the hematite-coated silica/solution spectra slightly longer acquisition time and spectral averaging were necessary to achieve a similar signal-to-noise ratio as the bare silica/solution spectra due to absorption losses of the excitation beam within the hematite film. During the course of the hematite wetting and dehydration experiments, spectra were collected in consecutive 10 s increments. The TIR-Raman spectra in the S-O stretching region have been background-subtracted to remove contributions from scatter arising from the bulk of the silica hemisphere and the hematite film to the detected spectra (see Supplementary material, Figs. S1–S3). The spectra of silica/water and hematite/water were checked at the beginning and end of each day that experiments were run to ensure system stability, reproducibility, and reversibility of ion adsorption.

All sulfate solutions were prepared by mixing the appropriate amount of  $MgSO_4$  ( $>99.5\%$  pure, powder, anhydrous, Fisher Scientific) with nanopure water (18.3 M $\Omega$ , NanoPure, Barnstead/ThermoFyne) to the desired concentration. To each solution enough NaCl ( $\geq 99.5\%$  pure, crystalline, anhydrous, Sigma-Aldrich) was added to have a 1 molal (m, mole solute/kg solvent) NaCl background electrolyte level. All salts were baked for 4 h at  $500^\circ\text{C}$  prior to use to remove organic contamination [49]. Solution pH was controlled by preparing solutions to the desired concentrations and then adding concentrated HCl (37% wt., Fisher, trace metal grade, Fisher Scientific) dropwise until the desired pH was reached. The added volume of HCl was small enough not to significantly change the solution concentration. The pH of solutions was monitored with a standard pH meter (Ag/AgCl glass electrode, Accumet AB15, Fisher Scientific) which had been calibrated following the procedure of Wiesner et al. for high ionic strength solutions [50]. All sample solutions were conditioned overnight at  $23^\circ\text{C}$  prior to use. In a typical TIR-Raman experiment the solution was prepared, conditioned, and then transferred to a clean solution reservoir where it was then pumped to the sample flow cell. Finally, the sample solution was allowed at least 15 min to equilibrate before spectra were acquired.

### 3. Results and discussion

#### 3.1. TIR-Raman spectra of bare and hematite-coated silica/sulfate solution interfaces

Shown in Fig. 3 are TIR-Raman control spectra for silica/MgSO<sub>4</sub> solution interfaces in the S–O stretching region as a function of pH and ion concentration. The sharp peak located at 980 cm<sup>-1</sup> is assigned to the symmetric stretch ( $\nu_{SS}$ -SO<sub>4</sub><sup>2-</sup>) of bulk solvated SO<sub>4</sub><sup>2-</sup> ions possessing T<sub>d</sub> symmetry. However, little signal intensity is observed for the triply degenerate  $\nu_{AS}$ -SO<sub>4</sub><sup>2-</sup> modes centered at 1100 cm<sup>-1</sup> in accordance with the weak Raman transition moment for these vibrations when sulfate possesses T<sub>d</sub> symmetry (Table 1) [20,51,52]. It is apparent that decreasing the pH from 8 to 1 has little effect on the overall spectral intensity detected (Fig. 3A–C). This is attributed to the ~100 nm probing depth at the silica/solution interface resulting in a detected TIR-Raman signal intensity primarily arising from bulk solvated SO<sub>4</sub><sup>2-</sup> ions relatively far from the interface. With lowering of the solution pH, the deep probing depth masks the effect of enhanced attractive electrostatic interactions between SO<sub>4</sub><sup>2-</sup> ions and the increasingly positively charged silica surface from the removal of negative silica surface charges (as the point-of-zero-charge (pzc) for silica is effectively ~2 [53,54]). However, even at the lowest pH value tested (pH 1, Fig. 3C), the TIR-Raman spectra resemble Raman spectra of freely solvated SO<sub>4</sub><sup>2-</sup> ions.

Fig. 4 presents the TIR-Raman spectra for the hematite-coated silica/MgSO<sub>4</sub> solution interfaces from pH 8 to pH 3 (Fig. 4A–C). Spectra for MgSO<sub>4</sub> solutions at pH 1 are not shown as the hematite film was not stable at this pH. Similar to results obtained at the silica/MgSO<sub>4</sub> solution interface (Fig. 3), the peak at ~980 cm<sup>-1</sup> is assigned to the  $\nu_{SS}$ -SO<sub>4</sub><sup>2-</sup> vibration. However, for the spectra shown in

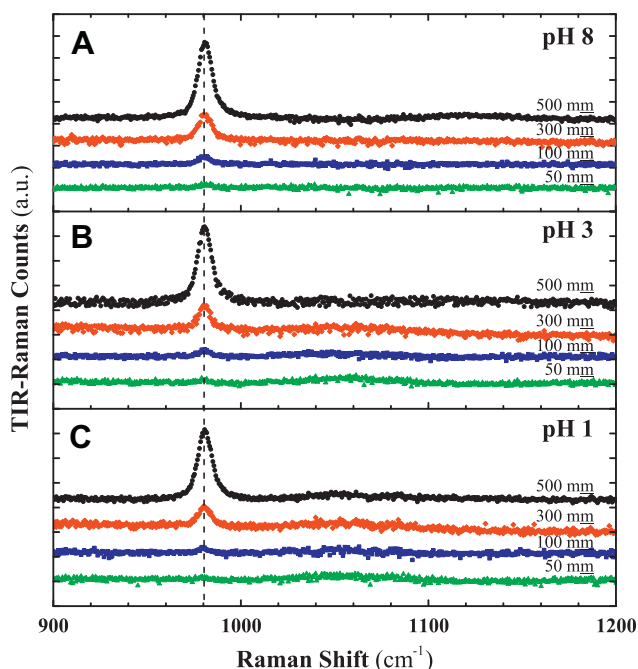


**Fig. 3.** TIR-Raman spectra of silica/MgSO<sub>4</sub> solution interfaces at (A) pH 8, (B) pH 3, and (C) pH 1 for 50 mM (green triangles), 100 mM (blue squares), 300 mM (red diamonds), and 500 mM (black circles) MgSO<sub>4</sub> solution concentrations. The sharp peak at 980 cm<sup>-1</sup> found in all spectra (except for the 50 mM solutions where this spectral feature is weak) is assigned to the  $\nu_{SS}$ -SO<sub>4</sub><sup>2-</sup> stretch of solvated SO<sub>4</sub><sup>2-</sup> ions possessing T<sub>d</sub> symmetry (dashed vertical line). All solutions include a 1 mM NaCl background electrolyte concentration. All spectra have been offset for clarity. (For interpretation of the references to color in this figure legend, the reader is referred to the web version of this article.)

Fig. 4 the peak at 980 cm<sup>-1</sup> features greater asymmetry than observed for the silica/MgSO<sub>4</sub> solution results (Fig. 3). The origin of this peak asymmetry is likely to be attributed to the presence of adsorbed SO<sub>4</sub><sup>2-</sup> ions on the hematite surface, analogous, but to a lesser extent, to observations made on the  $\nu_{SS}$ -SO<sub>4</sub><sup>2-</sup> peak frequency in Raman spectroscopy ion pairing studies [52,55]. Little variation is observed in the  $\nu_{SS}$ -SO<sub>4</sub><sup>2-</sup> peak asymmetry for spectra shown in Fig. 4 with a decrease in solution pH. This indicates that SO<sub>4</sub><sup>2-</sup> adsorption to the hematite surface is occurring even when the net surface charge is nearly zero (hematite pzc ~ 8) [4,53,54].

Also observed in Fig. 4 spectra is the broad spectral feature centered at ~1060 cm<sup>-1</sup> associated with the  $\nu_{AS}$ -SO<sub>4</sub><sup>2-</sup> stretching vibrations which increase in intensity with lowered pH. The presence of  $\nu_{AS}$ -SO<sub>4</sub><sup>2-</sup> vibrations in the hematite-coated silica/solution spectra further suggests that adsorbed SO<sub>4</sub><sup>2-</sup> ions are present and contributing to the TIR-Raman spectra. While the observed spectra in Fig. 4 lack the  $\nu_{AS}$ -SO<sub>4</sub><sup>2-</sup> peak characteristics associated with unambiguous adsorbed sulfate they are clearly different than the control spectra in Fig. 3 for the silica/solution interfaces where no adsorption is expected [5,20,56]. Ultimately, the spectra for the hematite-coated silica/MgSO<sub>4</sub> solution interfaces suggest that both freely solvated and adsorbed SO<sub>4</sub><sup>2-</sup> ions are contributing to the detected TIR-Raman signal intensity however the former contribution is the dominant one.

The inability to definitively assign an adsorption geometry for SO<sub>4</sub><sup>2-</sup> ions at the hematite surface from the TIR-Raman spectra presented in Fig. 4 is attributed to the penetration depth of the evanescent wave in these experiments which still reaches quite deep (~34 nm) into the bulk solution phase. Hence, the number density of solvated SO<sub>4</sub><sup>2-</sup> ions within this probing region will be much greater than that of SO<sub>4</sub><sup>2-</sup> ions adsorbed at the hematite surface. In contrast to ATR-IR results studying SO<sub>4</sub><sup>2-</sup> adsorption onto hematite surfaces that are able to distinguish clearer spectral differences between adsorbed and solution sulfate spectra, in this study we have a thin (~100 nm) film of hematite instead of a thick (~300 nm) packed colloid layer [5]. This is significant as in the TIR-Raman experiment the evanescent beam is generated at the hematite-coated silica/solution interface which results in only SO<sub>4</sub><sup>2-</sup> ions at the surface and the subsurface of the hematite film within the beam spot to contribute to the resulting spectra. In a typical ATR-IR experiment the evanescent beam is generated at the TIR-element/solution + colloid interface resulting in the beam interacting with the entire colloid layer, thus significantly increasing the signal-to-noise ratio [57].

#### 3.2. TIR-Raman spectra of wet and dehydrated hematite-coated silica/sulfate solution interfaces

It is reasonable to expect that if the majority of the solution is removed from the hematite-coated silica/solution interface then SO<sub>4</sub><sup>2-</sup> ions adsorbed on the surface of the hematite thin film would contribute to the detected signal intensity to a greater degree and a clearer picture of the ion binding geometry present should arise. Shown in Fig. 5 are TIR-Raman spectra of the hematite-coated silica/100 mM MgSO<sub>4</sub> solution interface at pH 8 where the film has been exposed to the solution for 15 min. Following this equilibration time the solution has been pumped out of the sample flow cell, thus leaving behind the hematite surface wetted only by a thin aqueous film of sulfate solution. Fig. 5A and B detail the time evolution of TIR-Raman spectra in the  $\nu_{SS}$ -SO<sub>4</sub><sup>2-</sup> and  $\nu_{AS}$ -SO<sub>4</sub><sup>2-</sup> stretching regions, respectively, of the wet hematite surface. Apparent in both Fig. 5A and B are the significant spectral changes which occur over time with SO<sub>4</sub><sup>2-</sup> adsorption on the wet hematite surface compared to the results for the immersed hematite-coated silica/solution spectra shown in Fig. 4. The spectra in Fig. 5 have been fit with Lorentzian functions to determine peak position, etc. and the

**Table 1**

List of symmetric and asymmetric peak frequencies for anhydrous and aqueous sulfates as well as for the hematite/sulfate solution interface.

System	Exptl. conditions	Method <sup>a</sup>	Peak frequency (cm <sup>-1</sup> )		Ref.
			$\nu_{SS}\text{-SO}_4^{2-}(\nu_1)$	$\nu_{AS}\text{-SO}_4^{2-}(\nu_3)$	
$\text{SO}_4^{2-}(\text{s})$	Ca <sup>2+</sup> , anhydrite crystal	Raman	1016	1110, 1128, 1160	[56]
	K <sup>+</sup> , grown crystal	Raman	985	1096, 1111, 1148	[59]
$\alpha\text{-Fe}_2\text{O}_3/\text{SO}_4^{2-}$ (evacuated)	Colloid layer	ex situ T-IR	950	1030, 1131, 1245	[60]
$\alpha\text{-Fe}_2\text{O}_3/\text{SO}_4^{2-}$ (air-dried)	Colloid layer	ex situ T-IR	970	1040, 1128, 1200	[60]
	mixed with KBr and compressed into disk	ex situ T-IR	950	1030, 1130, 1255	[62]
	Na <sup>+</sup>	DR-IR	~1020	1150, 1270, 1360	[61]
	20 $\mu\text{M}$ , pH 3.6, colloid layer	in situ ATR-IR	970	1047, 1135, 1195	[5]
$\alpha\text{-Fe}_2\text{O}_3/\text{SO}_4^{2-}(\text{aq})$ (wet)	Mg <sup>2+</sup> , 100 $\mu\text{M}$ (+1 $\mu\text{M}$ NaCl)	in situ TIR-Raman	977 ( $t = 10$ s)	~1063	This study
			977, 993 ( $t = 30$ s)	1072, 1125, 1195	This study
$\alpha\text{-Fe}_2\text{O}_3/\text{SO}_4^{2-}(\text{aq})$ (dry)	Mg <sup>2+</sup> , 100 $\mu\text{M}$ (+1 $\mu\text{M}$ NaCl)	in situ TIR-Raman	990 ( $t \geq 180$ s)	1097, 1129, 1149	This study
$\alpha\text{-Fe}_2\text{O}_3/\text{SO}_4^{2-}(\text{aq})$	pH 3, colloid layer	in situ ATR-IR	976	1060, 1128	[5]
	Na <sup>+</sup> , 50 $\mu\text{M}$ , pH 4, colloid layer	in situ ATR-IR	976	1008, 1055, 1130	[18]
	Mg <sup>2+</sup> , 100–500 $\mu\text{M}$ , pH 3–8, thin film	in situ TIR-Raman	980	~1060	This study
$\text{SO}_4^{2-}(\text{aq})$	Na <sup>+</sup> , Mg <sup>2+</sup> , sat. sln	Raman	980/985	1105/1120	[51]
	Na <sup>+</sup> , 0.1 M (+1 M NaCl)	Raman	982	~1110	[63]
	Mg <sup>2+</sup> , 0.5 $\mu\text{M}$ to 3 $\mu\text{M}$ , pH 5.95	Raman	980, 993, 1005	–	[52]
	10 mM, pH 5.5	Raman	–	1101	[5]

<sup>a</sup> ATR-IR, attenuated total reflection-infrared; DR-IR, diffuse reflectance-infrared; T-IR, transmission-infrared; TIR-Raman, total internal reflection-Raman.

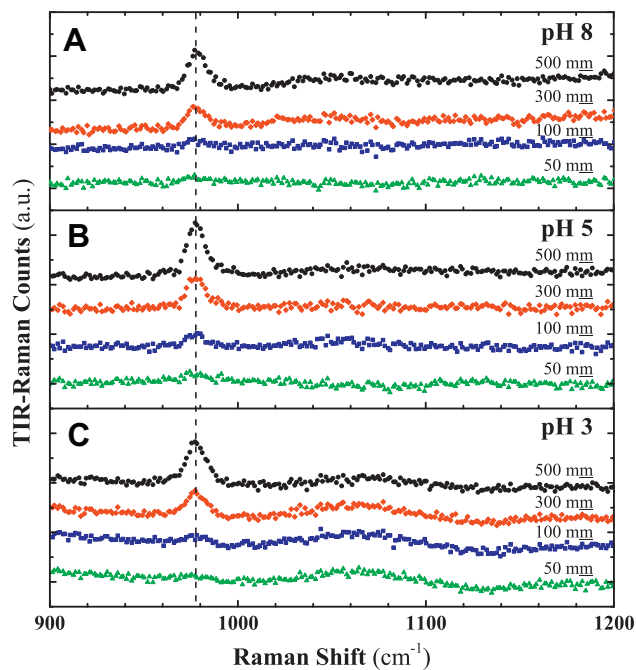


**Fig. 4.** TIR-Raman spectra of hematite/MgSO<sub>4</sub> solution interfaces at (A) pH 8, (B) pH 5, and (C) pH 3 for 50  $\mu\text{M}$  (green triangles), 100  $\mu\text{M}$  (blue squares), 300  $\mu\text{M}$  (red diamonds), and 500  $\mu\text{M}$  (black circles) MgSO<sub>4</sub> solution concentrations. The  $\nu_{SS}\text{-SO}_4^{2-}$  stretching peak at  $\sim 980$   $\text{cm}^{-1}$  is increasingly asymmetric with decreasing pH. This peak is assigned to solvated  $\text{SO}_4^{2-}$  ions possessing  $T_d$  symmetry as well as adsorbed  $\text{SO}_4^{2-}$  ions on the hematite surface (dashed vertical line). With decreasing pH the weak  $\nu_{AS}\text{-SO}_4^{2-}$  stretching modes centered at  $\sim 1060$   $\text{cm}^{-1}$  become more pronounced. All solutions include a 1  $\mu\text{M}$  NaCl background electrolyte concentration. All spectra have been offset for clarity. (For interpretation of the references to color in this figure legend, the reader is referred to the web version of this article.)

fitting parameters may be found in the [Supplementary material](#) (Table S1). Here it is important to note that for the TIR-Raman of the wet hematite surface, as shown in Fig. 5, the absolute intensities of the peak components are not reproducible between spectral

runs. This is attributed to the uncontrollable and heterogeneous nature of the hematite film drying. However, general trends are reproduced between spectral acquisitions for these experiments and these form the basis for our interpretation.

The initial spectrum ( $t = 10$  s) in Fig. 5A resembles the hematite-coated silica/solution spectra shown in Fig. 4 where the main spectral feature centered at 977  $\text{cm}^{-1}$  is again assigned to the  $\nu_{SS}\text{-SO}_4^{2-}$  stretching mode of  $\text{SO}_4^{2-}$  ions possessing  $T_d$  symmetry. By  $t = 30$  s, while there is still a peak component at 977  $\text{cm}^{-1}$ , the spectrum is dominated by a new peak at 993  $\text{cm}^{-1}$  assigned to inner-sphere adsorbed sulfate ions of unknown coordination structure at the hematite surface. As time progresses large spectral changes are observed in Fig. 5A where as many as four peak frequencies for the  $\nu_{SS}\text{-SO}_4^{2-}$  stretching mode are observed (Table 1) which correspond to sulfate in differing molecular environments. The observed spectral changes are the result of the complex and varying molecular environments experienced by sulfate anions at the hematite surface as the film dries. These environments most likely range from freely solvated (or hydrogen-bound)  $\text{SO}_4^{2-}$  ions (peak component at 977  $\text{cm}^{-1}$  observed at  $t = 10$  s), to inner-sphere adsorbed  $\text{SO}_4^{2-}$  ions (peak components at 988  $\text{cm}^{-1}$  and 993  $\text{cm}^{-1}$  for  $50 \text{ s} < t < 90$  s) and finally to dry MgSO<sub>4</sub> particles at the surface (peak component at 990  $\text{cm}^{-1}$  observed for  $t = 300$  s), in accordance with observations for anhydrous crystalline sulfate salts [20,56]. While some studies have suggested the protonation of adsorbed  $\text{SO}_4^{2-}$  ions on hematite surfaces to form surface-bound bisulfate ( $\text{HSO}_4^-$ ) complexes upon drying only faint evidence for this can be seen in our spectra at times  $t = 30$  s and 40 s [5,18]. The weak peak at 1042  $\text{cm}^{-1}$  in the above referenced spectra is generally attributed to the  $\nu_{SS}\text{-SO}_3$  mode of adsorbed  $\text{HSO}_4^-$  ion complexes [58].

The spectra in Fig. 5A reveal the existence of adsorbed  $\text{SO}_4^{2-}$  ions at the hematite-coated silica/solution interface and the complex molecular rearrangements that occur as the hematite surface dries. However, the spectra in the asymmetric S–O stretching region are needed because those in the symmetric region are insufficient to definitively ascertain the binding mode of the sulfate ions at the hematite surface. This is due to the minor frequency differences

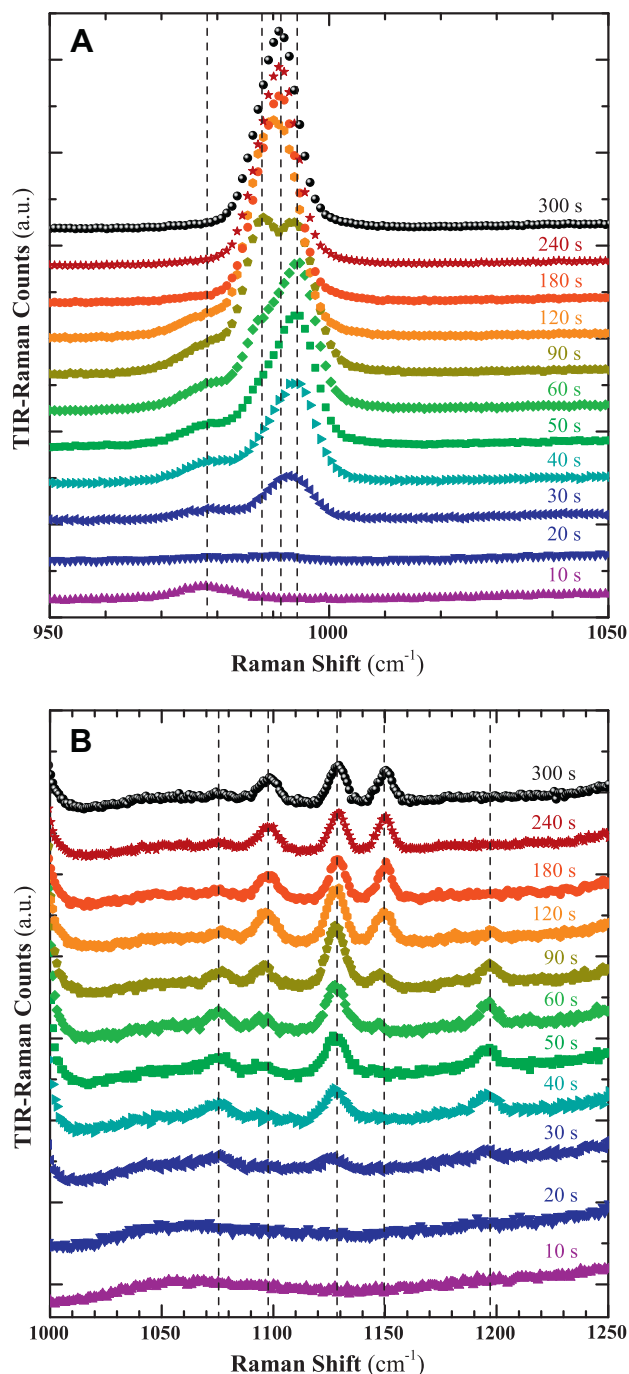


**Fig. 5.** Time evolution of TIR-Raman spectra in the (A)  $\nu_{SS}\text{-SO}_4^{2-}$  and (B)  $\nu_{AS}\text{-SO}_4^{2-}$  stretching regions of the wetted hematite film after removal of a pH 8 100 mM  $\text{MgSO}_4$  solution with 1 M NaCl background electrolyte concentration. Spectra were collected immediately following solution removal in 10 s intervals for a total time of 5 min. Positions of peak centers are shown by dashed vertical lines. All spectra have been offset for clarity.

expected for the  $\nu_{SS}\text{-SO}_4^{2-}$  modes between the various molecular environments present at the hematite surface.

By examining the  $\nu_{AS}\text{-SO}_4^{2-}$  peak behavior, a clearer picture of the sulfate adsorbate structures present at the hematite surface is revealed. As seen from the time evolution of the TIR-Raman spectra of the wet hematite surface in the  $\nu_{AS}\text{-SO}_4^{2-}$  region (Fig. 5B), three asymmetric stretching peaks at 1072  $\text{cm}^{-1}$ , 1125  $\text{cm}^{-1}$ , and 1195  $\text{cm}^{-1}$  appeared at  $t = 30$  s. As drying continues two other peaks at 1096  $\text{cm}^{-1}$  and 1148  $\text{cm}^{-1}$  are observed

in the spectra beginning at  $t = 60$  s. Finally, at  $t > 180$  s the spectral components at 1072  $\text{cm}^{-1}$  and 1195  $\text{cm}^{-1}$  have disappeared and the spectra resemble Raman spectra of anhydrous sulfate salts indicating complete drying of the hematite film after 120 s [20,59].

The appearance of three asymmetric stretching modes in the TIR-Raman spectra shown in Fig. 5B indicates that the  $\text{SO}_4^{2-}$  ions are adsorbing to the hematite surface in a bidentate inner-sphere fashion congruent with a symmetry lowering from  $T_d$  to  $C_{2v}$ . In contrast, most previous *in situ* ATR-IR studies have only observed two  $\nu_{AS}\text{-SO}_4^{2-}$  modes and consequently inner-sphere monodentate sulfate binding to hematite was suggested [5,33]. While a symmetry argument may not be completely appropriate for a constrained environment such as a surface, in this case it allows a simple picture of  $\text{SO}_4^{2-}$  adsorption to be drawn [18].

An argument could also be made that the TIR-Raman results presented in Fig. 5 are not truly representative of the oxide film/ aqueous solution interface as the sulfate solution has been removed; however, if  $\text{SO}_4^{2-}$  ions were adsorbing in a monodentate inner-sphere fashion at the hematite surface this would be very apparent in our spectra, that is, only peaks at  $\sim 980$ ,  $\sim 1060$  and  $\sim 1130$   $\text{cm}^{-1}$  would be expected to appear. This is not the case. Also of note is that the results presented in Fig. 5 are not simply drying experiments as the hematite film still has an aqueous film of  $\text{MgSO}_4$  solution on its surface for at least  $\sim 2$  min following solution removal. Previously reported drying experiments have generally proposed a bidentate adsorption structure for sulfate at hematite surfaces following an IR analysis of colloidal hematite which had been exposed to sulfate solution, and then either air-dried [5,60,61], evacuated [60], or air-dried and pressed into a KBr pellet [62]. These data and spectral assignments are given in Table 1. While at later times ( $t > 120$  s), TIR-Raman spectra do indeed resemble conventional Raman spectra of dry sulfate salts, spectra taken at intermediate times clearly differ indicating that adsorbed sulfate ions, not dry particles, are dominating the spectra.

In rationalizing the results presented in Fig. 5B, which indicate bidentate inner-sphere adsorption geometry for sulfate at the hematite surface, it is necessary to consider possible spectral contributions from non-adsorbed sulfate species. The Raman transition moment strengths for the  $\nu_{AS}\text{-SO}_4^{2-}$  vibrations of  $\text{SO}_4^{2-}$  ions with  $T_d$  symmetry, or freely solvated  $\text{SO}_4^{2-}$  ions, are quite low; this is apparent for spectra shown in Fig. 3 where no  $\text{SO}_4^{2-}$  adsorption should be present. In comparison, with IR spectroscopy, the peak strength for the triply degenerate  $\nu_{AS}\text{-SO}_4^{2-}$  modes of freely solvated  $\text{SO}_4^{2-}$  ions are both broad and strong [20,58]. This indicates that ATR-IR spectra examining  $\text{SO}_4^{2-}$  adsorption could have spectral convolutions from  $\text{SO}_4^{2-}$  ions within the probe spot but which are not adsorbed. In that case it is reasonable to believe that the broad, strong  $\nu_{AS}\text{-SO}_4^{2-}$  peak from solvated  $\text{SO}_4^{2-}$  ions could obscure weaker modes associated with a bidentate adsorption structures. This could potentially explain the conflicting assignments present in the ATR-IR literature with regards to  $\text{SO}_4^{2-}$  adsorption structures at the hematite surface.

Another plausible reason for the discrepancies between the inner-sphere adsorption geometries found using TIR-Raman versus ATR-IR methods could be the influence of hematite surface structure, i.e. the surface terminations of the hematite crystal unit cell, on anion binding as this is known to influence adsorption motifs [64]. Recently Rubasinghege et al. [43] demonstrated different adsorption geometries for sulfate anions onto hematite particles as a function of particle scale (microrods versus nanorods) which dictated the hematite surface terminations present. While Rubasinghege et al.'s findings could possibly explain why the results from this study differ from various ATR-IR findings as in this study the hematite phase is a uniform thin film versus a packed colloidal layer, an analysis of the surface terminations present on the hematite film is beyond the scope of the present study.

#### 4. Conclusions

In this study TIR-Raman spectroscopy, a surface-sensitive technique, was used to examine  $\text{SO}_4^{2-}$  ion behavior at the buried hematite-coated silica/solution interface as well as the influence that solution removal had for the sulfate anion. To our knowledge, this is the first time that TIR-Raman spectroscopy has been applied to study simple, inorganic anion adsorption onto oxide mineral surfaces and demonstrates the potential of this technique to investigate such systems. Results for the hematite-coated silica/ $\text{MgSO}_4$  solution interface indicate that sulfate adsorption increases with a decrease in pH, as expected. Moreover, bidentate inner-sphere adsorption is dominant.

With removal of the bulk solution clear spectral signatures of sulfate adsorption are observed in the TIR-Raman spectra of the wet hematite surface. While the spectral features corresponding to  $\nu_{\text{SS}}\text{-SO}_4^{2-}$  stretching vibrations demonstrate the complex molecular rearrangement that adsorbed  $\text{SO}_4^{2-}$  ions undergo during drying, the  $\nu_{\text{AS}}\text{-SO}_4^{2-}$  stretching modes indicate that inner-sphere  $\text{SO}_4^{2-}$  adsorption onto the hematite surface occurs primarily in a bidentate geometry. This finding agrees with the results of Paul et al. [18] in contrast to most inner-sphere adsorption structures previously proposed for  $\text{SO}_4^{2-}$  at hematite surfaces from observations using in situ ATR-IR spectroscopy. The results presented here are significant as they may necessitate rethinking of adsorption models which predict monodentate inner-sphere adsorption of sulfate onto hematite [8]. While the results presented in this study are very promising there is much room for improvement in the development and application of TIR-Raman spectroscopy to study ion adsorption onto mineral surfaces.

#### Acknowledgments

A.M. Jubb, D. Verreault, L.J. Criscenti, L.E. Katz, and H.C. Allen acknowledge the DOE-BES Geochemistry (AMJ, DV, HCA: #DE-FG02-04ER15495; LJC/Sandia: #DE-AC04-94AL85000; LEK, #DE-FG02-04ER15496) for funding this work. R. Posner gratefully acknowledges financial support provided by a Feodor-Lynen-Fellowship of the Alexander-von-Humboldt Foundation and The Ohio State University. Sandia National Laboratories is a multi-program laboratory managed and operated by Sandia Corporation, a wholly owned subsidiary of Lockheed Martin Corporation, for the U.S. Department of Energy's National Nuclear Security Administration under contract DE-AC04-94AL85000.

#### Appendix A. Supplementary material

Supplementary data associated with this article can be found, in the online version, at <http://dx.doi.org/10.1016/j.jcis.2013.02.031>.

#### References

- [1] D. Langmuir, *Aqueous Environmental Geochemistry*, first ed., Prentice Hall, Upper Saddle River, New Jersey, 1997.
- [2] C.R. Usher, A.E. Michel, V.H. Grassian, *Chem. Rev.* 103 (2003) 4883.
- [3] D.J. Cziczko, K.D. Froyd, S.J. Gallavardin, O. Moehler, S. Benz, H. Saathoff, D.M. Murphy, *Environ. Res. Lett.* 4 (2009) 044013.
- [4] R.M. Cornell, U. Schwertmann, *The Iron Oxides: Structure, Properties, Reactions, Occurrences and Uses*, second ed., Wiley-VCH, Weinheim, Germany, 2003.
- [5] S.J. Hug, *J. Colloid Interface Sci.* 188 (1997) 415.
- [6] G. Lefèvre, *Adv. Colloid Interface Sci.* 107 (2004) 109.
- [7] G.E. Brown, V.E. Henrich, W.H. Casey, D.L. Clark, C. Eggleston, A. Felmy, D.W. Goodman, M. Grätzel, G. Maciel, M.I. McCarthy, K.H. Nealson, D.A. Sverjensky, M.F. Toney, J.M. Zachara, *Chem. Rev.* 99 (1999) 77.
- [8] K. Fukushi, D.A. Sverjensky, *Geochim. Cosmochim. Acta* 71 (2007) 1.
- [9] R.P.J.J. Rietra, T. Hiemstra, W.H. van Riemsdijk, *Geochim. Cosmochim. Acta* 63 (1999) 3009.
- [10] R.P.J.J. Rietra, T. Hiemstra, W.H. van Riemsdijk, *J. Colloid Interface Sci.* 218 (1999) 511.
- [11] K.F. Hayes, C. Papelis, J.O. Leckie, *J. Colloid Interface Sci.* 125 (1988) 717.
- [12] J.R. Rustad, E. Wasserman, A.R. Felmy, *Surf. Sci.* 424 (1999) 28.
- [13] T.P. Trainor, A.M. Chaka, P.J. Eng, M. Newville, G.A. Waychunas, J.G. Catalano, G.E. Brown Jr., *Surf. Sci.* 573 (2004) 204.
- [14] C.S. Lo, K.S. Tanwar, A.M. Chaka, T.P. Trainor, *Phys. Rev. B* 75 (2007). 075425-1 (Errata: *Phys. Rev. B* 75 (2007) 209901-1).
- [15] F.J. Millero, *Chemical Oceanography*, third ed., CRC Press, Boca Raton, FL, 2005.
- [16] D.K. Nordstrom, C.N. Alpers, C.J. Ptacek, D.W. Blowes, *Environ. Sci. Technol.* 34 (2000) 254.
- [17] B.J. Finlayson-Pitts, J.N. Pitts Jr., *Chemistry of the Upper and Lower Atmosphere: Theory, Experiments and Applications*, Academic Press, San Diego, CA, 2000.
- [18] K.W. Paul, M.J. Borda, J.D. Kubicki, D.L. Sparks, *Langmuir* 21 (2005) 11071.
- [19] K. Müller, G. Lefèvre, *Langmuir* 27 (2011) 6830.
- [20] A.M. Jubb, H.C. Allen, *J. Phys. Chem. C* 116 (2012) 9085.
- [21] J.D. Ostergren, G.E. Brown, G.A. Parks, P. Persson, *J. Colloid Interface Sci.* 225 (2000) 483.
- [22] E.J. Elzinga, D.L. Sparks, *J. Colloid Interface Sci.* 308 (2007) 53.
- [23] P.J. Swedlund, J.G. Webster, G.M. Miskelly, *Geochim. Cosmochim. Acta* 73 (2009) 1548.
- [24] A.W. Rose, G.C. Bianchi-Mosquera, *Econ. Geol.* 88 (1993) 1226.
- [25] Z. Yang, A.K. Bertram, K.C. Chou, *J. Phys. Chem. Lett.* 2 (2011) 1232.
- [26] M. Claeys, W. Wang, A.C. Ion, I. Kourtev, A. Gelencsér, W. Maenhaut, *Atmos. Environ.* 38 (2004) 4093.
- [27] O. Böge, Y. Miao, A. Plewka, H. Herrmann, *Atmos. Environ.* 40 (2006) 2501.
- [28] S.C.B. Myneni, X-ray and vibrational spectroscopy of sulfate in earth materials, in: C.N. Alpers, J.L. Jambor, D.K. Nordstrom (Eds.), *Sulfate Minerals – Crystallography, Geochemistry and Environmental Significance*, vol. 40, Mineralogical Society of America, Washington, DC, 2000, p. 113.
- [29] G. Lefèvre, M. Fédoroff, *Phys. Chem. Earth* 31 (2006) 499.
- [30] D. Peak, D.L. Sparks, *Environ. Sci. Technol.* 36 (2002) 1460.
- [31] C.C. Chen, M.L. Coleman, L.E. Katz, *Environ. Sci. Technol.* 40 (2006) 142.
- [32] C.J. Landry, C.M. Koretsky, T.J. Lund, M. Schaller, S. Das, *Geochim. Cosmochim. Acta* 73 (2009) 3723.
- [33] C.M. Eggleston, S. Hug, W. Stumm, B. Sulzberger, M. Dos Santos Afonso, *Geochim. Cosmochim. Acta* 62 (1998) 585.
- [34] N.J. Harrick, *Internal Reflection Spectroscopy*, Wiley, New York, 1967.
- [35] M. Born, E. Wolf, *Principles of Optics*, seventh ed., Cambridge University Press, Cambridge, United Kingdom, 1999.
- [36] E. Tyrode, M.W. Rutland, C.D. Bain, *J. Am. Chem. Soc.* 130 (2008) 17434.
- [37] M. Milosevic, *Internal Reflection and ATR Spectroscopy*, Wiley, New York, 2012.
- [38] D.A. Beattie, M. Lidström Larsson, A.R. Holmgren, *Vib. Spectrosc.* 41 (2006) 198.
- [39] P.R. Greene, C.D. Bain, *Colloids Surf., B* 45 (2005) 174.
- [40] D.A. Woods, J. Petkov, C.D. Bain, *J. Phys. Chem. B* 115 (2011) 7341.
- [41] P.R. Greene, C.D. Bain, *Spectrosc. Eur.* 16 (2004) 8.
- [42] D.A. Woods, C.D. Bain, *Analyst* 137 (2012) 35.
- [43] G. Rubasinghege, R.W. Lentz, M.M. Scherer, V.H. Grassian, *Proc. Natl. Acad. Sci. USA* 107 (2010) 6628.
- [44] K. Mörl, U. Röpke, B. Knappe, J. Lehmann, R. Perthel, H. Schröder, *Thin Solid Films* 60 (1979) 49.
- [45] J.A. Glasscock, P.R.F. Barnes, I.C. Plumb, A. Bendavid, P.J. Martin, *Thin Solid Films* 516 (2008) 1716.
- [46] L. Zhang, W. Liu, Y.R. Shen, D.G. Cahill, *J. Phys. Chem. C* 111 (2007) 2069.
- [47] A.M. Jubb, H.C. Allen, *ACS Appl. Mater. Interfaces* 2 (2010) 2804.
- [48] D.L.A. de Faria, S. Venncio Silva, M.T. de Oliveira, *J. Raman Spectrosc.* 28 (1997) 873.
- [49] W. Hua, A.M. Jubb, H.C. Allen, *J. Phys. Chem. Lett.* 2 (2011) 2515.
- [50] A.D. Wiesner, L.E. Katz, C.C. Chen, *J. Colloid Interface Sci.* 301 (2006) 329.
- [51] R.E. Hester, R.A. Plane, *Inorg. Chem.* 3 (1964) 769.
- [52] W.W. Rudolph, G. Irmer, G.T. Hefter, *Phys. Chem. Chem. Phys.* 5 (2003) 5253.
- [53] G.A. Parks, *Chem. Rev.* 65 (1965) 177.
- [54] M. Kosmulski, *Surface Charging and Points of Zero Charge*, CRC Press, Boca Raton, 2009.
- [55] Y.-H. Zhang, C.K. Chan, *J. Phys. Chem. A* 104 (2000) 9191.
- [56] B.J. Berenblut, P. Dawson, G.R. Wilkinson, *Spectrochim. Acta* 29A (1973) 29.
- [57] S.J. Hug, B. Sulzberger, *Langmuir* 10 (1994) 3587.
- [58] A.M. Jubb, H.C. Allen, *J. Phys. Chem. C* 116 (2012) 13161.
- [59] D. Liu, H.M. Lu, J.R. Hardy, F.G. Ullman, *Phys. Rev. B* 44 (1991) 7387.
- [60] R.L. Parfitt, R.S.C. Smart, *Soil Sci. Soc. Am. J.* 42 (1978) 48.
- [61] H. Watanabe, C.D. Gutleben, J. Seto, *Solid State Ionics* 69 (1994) 29.
- [62] L.J. Turner, J.R. Kramer, *Soil Sci.* 152 (1991) 226.
- [63] F.P. Daly, C.W. Brown, D.R. Kester, *J. Phys. Chem.* 76 (1972) 3664.
- [64] J.-F. Boily, *J. Phys. Chem. C* 116 (2012) 4714.